THE JOURNAL OF PHYSICAL CHEMISTRY C

ARTICLE

pubs.acs.org/JPCC

Safranine-T Triplet-State Quenching by Modified Silica Nanoparticles

Valeria B. Arce,[†,‡] Sonia G. Bertolotti,[§] Fernando J. V. E. Oliveira,[⊥] Claudio Airoldi,[¶] Mónica C. Gonzalez,[†] Patricia E. Allegretti,[‡] and Daniel O. Mártire*[,†]

[†]Instituto de Investigaciones Fisicoquímicas Teóricas y Aplicadas (INIFTA), Universidad Nacional de La Plata, Casilla de Correo 16, Sucursal 4, (1900) La Plata, Argentina

[‡]LADECOR, Departamento de Química, Facultad de Ciencias Exactas, Universidad Nacional de La Plata, La Plata, Argentina

[§]Departamento de Química, Universidad Nacional de Río Cuarto, 5800 Río Cuarto, Argentina

[⊥]Departamento de Química, CCEN, Universidade Federal da Paraíba (UFPB), 58059-900 João Pessoa, Paraíba, Brazil

[¶]Chemistry Institute, University of Campinas, P.O. Box 6154, 13084-971 Campinas, São Paulo, Brazil.

Supporting Information

ABSTRACT: Modified silica nanoparticles (NPs) were obtained by esterification of the silanol groups of fumed silica nanoparticles with 4-hydroxymethyl-*N*,*N*-dimethylbenzenamine. These particles were characterized by Fourier transform infrared spectroscopy, ^{13}C and ^{29}Si nuclear magnetic resonance, thermogravimetry, X-ray photoelectron spectroscopy, transmission electron microscopy with energy-dispersive spectroscopy, and measurement of the specific surface area. Laser flash photolysis experiments at the excitation wavelength of 532 nm were performed with safranine-T and NP suspensions in acetonitrile. Comparative experiments of safranine-T with solutions of 4-hydroxymethyl-*N*,*N*-dimethylbenzenamine and two other related alcohols were performed. Evidence for the triplet safranine-T H-abstraction from the organic group of the particles is obtained. The electron transfer from the organic group to the triplet excited states of safranine-T also takes place, as shown by the absorption traces obtained at 50 μs after the laser shot.

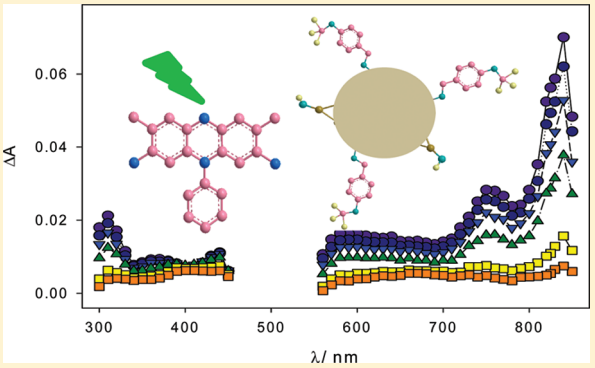

INTRODUCTION

As the nanotechnology industry grows, both the number of manufactured nanomaterials and their uses rise tremendously. Naturally occurring nanoscale materials are also ubiquitous in the biosphere, likely playing an important role in ecosystem dynamics.[1,2]

It is widely recognized in the literature that the adsorption−desorption dynamics of pollutants on suspended particles affects the chemical fate, toxicity, transport, and the efficiency of most remediation technologies.[3] Because slow desorption rates (in time scales on the order of months) are observed for most hydrophobic pollutants, photochemical and kinetic investigations of adsorbed pollutants on colloids are of importance to understanding environmental chemistry.

Chemical adsorption of organic compounds, such as alcohols, on the silica surface of sediments and on silica-based natural or manufactured nanomaterials in contaminated waters is a relevant process in the environment.[1]

Benzyl alcohol and its derivatives have many industrial applications.[4] Thus, synthetic silica nanoparticles chemically modified with benzyl alcohol derivatives are good models for hybrid materials formed by sorption of the alcohols to the silica particles in contaminated natural waters. On the other hand, pigments and dyes are widely used in the textile and leather-dyeing, paper, printing, pharmaceutical, and cosmetic industries.[5] Therefore, coadsorption of dyes and alcohols on surface particles[6] may have unprecedented consequences, as dyes are good absorbers of sunlight and may, therefore, initiate the depletion of adsorbed contaminants.

We here prepared fumed silica nanoparticles (NPs) functionalized with the benzyl alcohol derivative 4-hydroxymethyl-*N*,*N*-dimethylbenzenamine (DMB). While fumed silica has been used as a model support for studying the photophysics at gas/solid interfaces, few studies of the photophysics at solution/dispersed particle interfaces have appeared in the literature.[7−9] Thus, NP suspensions containing safranine-T were used to investigate the formation of organic radicals attached to the nanoparticles in laser flash photolysis experiments. Comparative experiments with solutions of DMB and other related compounds were also performed.

MATERIALS AND METHODS

Materials. Fumed silica (Sigma, specific surface area (SSA) of 390 ± 40 $m^2\ g^{-1}$ with an estimated particle diameter of 7 nm)

Received: May 31, 2011
Revised: August 10, 2011
Published: August 11, 2011

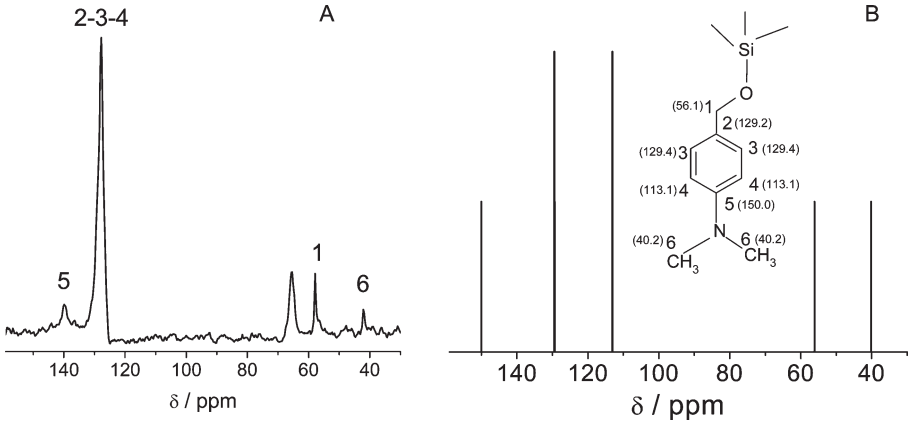

Figure 1. (A) ^{13}C NMR solid-state spectra for NPs. (B) Simulation of the spectrum shown in (A).

was dried in a crucible for 15 h at 120 °C and then in a muffle for 3 h at 250 °C and stored in a desiccator. *o*-Xylene was distilled onto molecular sieves (dried at 250 °C for 4 h), and DMB was obtained by the Cannizzaro reaction.[10] Ethyl acetate (Ciccarelli, p.a.), CaH_2 (Fluka), and $CaCl_2$ (Sigma-Aldrich) were used without further purification. Safranine-T chloride from Aldrich was recrystallized from ethanol before used. Distilled water (>18 MΩ·cm, <20 ppb of organic carbon) was obtained from a Millipore (Bedford, MA) system.

Synthesis of the Nanoparticles. We employed here a modification of the procedures used in the literature to derivatize silica nanoparticles with other alcohols.[11−14] A mixture of 5.30 g of DMB and 3.0 g of silica in 180 mL of *o*-xylene was refluxed during 38 h in a continuous solid−liquid extractor containing CaH_2 and a condenser with an anhydrous $CaCl_2$ drying tube. The heating rate was carefully regulated to obtain a continuous and stable flow of *o*-xylene through the extractor.

The products were filtered through an HPLC filtration device with 20 nm nylon filters, washed with 50 mL of hot *o*-xylene and finally with 50 mL of ethyl acetate. The resulting gel was first dried at 0.1 Torr and at room temperature for 3 h and then at 120 °C for 5 h. A white powder was obtained.

Infrared Spectroscopy. Fourier transform infrared (FTIR) spectra in the range from 4000 to 400 cm^{-1} were recorded on a Bruker EQUINOX 55 apparatus with a resolution of 2 cm^{-1}, using KBr disks. To achieve a high signal-to-noise ratio, 128 scans were accumulated for each sample.

Nitrogen Adsorption. Nitrogen adsorption isotherms were obtained using a gas adsorption apparatus (Micromeritics ASAP 2020 V1.04 E). The specific surface area (SSA) was evaluated by means of the Brunauer−Emmett−Teller (BET) equation,[8] considering a five-point isotherm in the reduced pressure range from 0.04 to 0.12 and assuming the surface area occupied by one nitrogen molecule to be 0.1620 nm^2.

Nuclear Magnetic Resonance. Nuclear magnetic resonance (NMR) spectra were obtained with a Bruker Avance II 400 spectrometer at room temperature, by assaying approximately 1 g of the solid sample compacted into a 7 mm zirconium oxide rotor. The measurements were performed at 75.47 and 59.61 MHz for carbon and silicon nuclei, with a magic-angle spinning (MAS) technique at 10 kHz. To increase the signal-to-noise ratio, the cross-polarization (CP) technique was applied. NMR spectra of ^{13}C and ^{29}Si were obtained with a pulse repetition of 1 and 3 s and contact times of 1 and 3 ms, respectively.

Thermogravimetry. The thermogravimetric curve was performed with a Shimadzu TGA-50 unit at a heating rate of 5 °C/min and a nitrogen flow of 50 mL/min. The instrument was calibrated with $CaC_2O_4 \cdot H_2O$.

Photoelectron Spectroscopy. The X-ray photoelectron spectroscopy (XPS) spectra were obtained under ultrahigh vacuum with an XR50 Specs GmbH spectrometer with Mg K(α) as the excitation source and a PHOIBOS 100 half-sphere energy analyzer. Calibration was performed with Au $4f_{7/2}$ and Cu $2p_{3/2}$ with binding energies of 84.00 and 933.67 eV, respectively.

Transmission Electron Microscopy. The transmission electron microscopy (TEM) images were obtained in a Philips CM 200 instrument equipped with an ultratwin objective lens and an acceleration voltage of 200 kV. The results obtained from SiO_2 or NP suspensions (see TEM images of NPs in Figure S1 in the Supporting Information) yielded aggregated nanoparticles of individual average diameters of 7 nm, in agreement with the data provided by the supplier for the bare silica particles. The microscope is equipped with an energy-dispersive spectroscopy (EDS) module.

Laser Flash Photolysis. Laser flash photolysis (LFP) experiments were performed by excitation with the second harmonic (532 nm) of a Nd:YAG Spectron SL 400 laser (18 ns fwhm). The instrumentation has been described elsewere.[15] The detection comprises a PTI monochromator coupled to a photomultiplier tube R666 Hamamatsu attached to a digital oscilloscope (HP54504). The laser beam was defocused to cover the full optical path of the beam scanner (10 mm) from a 150 W xenon lamp.

RESULTS AND DISCUSSION

Characterization of NPs. NMR spectra for silicon and carbon nuclei in the solid state provide information related to the silica network (see Figure S2 in the Supporting Information). The observed signals at −110, −99, and −91 ppm are assigned to $Si(OSi)_4$, Q^4; $Si(OSi)_3OH$, Q^3; and $Si(OSi)_2(OH)_2$, Q^2 chemical species,[16,17] respectively. Although a low signal-to-noise ratio is observed, it is possible to detect the typical species from the silica framework due to silanol and siloxane bonding. However, relationships involving these chemical sites are not conclusive, due to the fact that the CP-MAS technique does not provide quantitative information regarding the signal areas.

Table 1. Specific Surface Area (SSA), Decrease of SSA with Respect to the Bare SiO_2 Nanoparticles (ΔSSA), and Fraction of Functionalized Silanol Groups, *f*(SiOR)

sample	SSA (m^2 g^{-1})	ΔSSA (m^2 g^{-1})[b]	*f*(SiOR)[b,c]
NP	257 ± 1	133 ± 40	0.34 ± 0.18
SiO_2	390 ± 40[a]	0	0

[a] Provided by the supplier. [b] Error bars calculated from the propagation of the error bars in SSA. [c] Calculated as ΔSSA/390 m^2 g^{-1}.

For the NP sample (Figure 1), five distinct ^{13}C NMR signals were observed, as expected from the structure. Spectral simulations performed with ChemDraw Ultra 8.0, Cambridge Software, confirm the present attributions.

The spectrum shows two sets of signals for different chemical environments in the aromatic ring, corresponding to two to four carbon atoms located at 129.0 ppm and another peak at 140.0 ppm, respectively. The signal at 57.8 is attributed to carbon number 1 and the peak at 42.2 ppm is assigned to the methyl carbons attached to nitrogen, which supports the effectiveness of the nanoparticle's functionalization, as shown in Figure 1.

The lone pair of electrons of the N atom increases the electronic density of the aromatic ring of the particles. Thus, if the N atom acts as a H-bond acceptor from the silanol groups of the particle, the electronic density in the aromatic ring is expected to decrease. It would also be reasonable to expect a concomitant decrease of the difference in the shifts of the aromatic carbon atoms 3 with respect to carbon atoms 4 (Figure 1A). This explains the difference between the experimental ^{13}C NMR spectra of the particles and those simulated for the isolated molecule (Figure 1B).

The experimental spectrum shows two peaks at 57.8 and 65.4 ppm. The simulation of the free alcohol (result not shown) predicts a shift of 68.5 ppm for the carbon atom attached to the OH group, and the observed peak at 57.8 ppm is assigned to carbon 1 (see Figure 1). This result indicates that the sample contains both chemically and physically sorbed alcohol to the silica surface.

The decrease in SSA upon silica functionalization with the organic groups was observed for different systems.[18−21] The nitrogen molecule's adsorption, which preferentially takes place on the silanol groups, is partially precluded as the silica is chemically modified. Thus, functionalization of the silica nanoparticles results in a decrease in surface area.[22] From the SSA data, it is possible to obtain the fraction of modified silanol groups, *f*(SiOR), by neglecting the nitrogen adsorption on the functionalized silanols. These data are included in Table 1.

The mass of one bare SiO_2 nanoparticle (3.95×10^{-19} g) is calculated from the average volume of the nanoparticle and the density of silica (2200 kg m^{-3}).[23] The average number of silanol groups in one nanoparticle of bare SiO_2 estimated assuming spherical particles of radius r = 3.5 nm and 4.9 OH groups/nm^2[24] is 708. From these data and *f*(SiOR), the percentage of organic groups (%OG, w/w = 12 ± 4) is calculated.

Three decomposition steps were observed for the NP thermogravimetric curve: (i) room temperature to 200 °C, (ii) this temperature to 700 °C, and (iii) to end at 900 °C. The first step is associated with the elimination of the remaining washing solvents, *o*-xylene and mainly ethyl acetate. This solvent easily interacts with available surface silanol groups through hydrogen-bond formation. The second step is related to the thermal

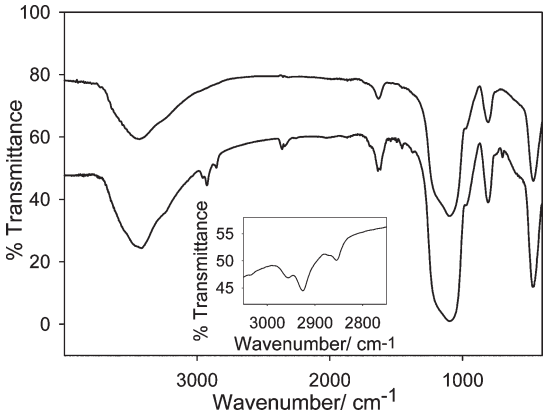

Figure 2. FTIR spectra of activated silica (upper trace) and modified silica (lower trace). Inset: expanded FTIR spectrum of modified silica.

decomposition of the organic moiety bonded to silica,[25] and the last stage corresponds to the remaining silanol condensation, to give the siloxane units.[26] The value of %OG calculated for NP from thermogravimetry (7%) is slightly lower than that obtained from the SSA [(12 ± 4)%] measurements. This could be due to the high content of organic solvents, which could cause the involvement of some organic moieties in its decomposition. In general, the good agreement between the values of %OG calculated from both methods is indicative of the involvement of one silanol group per alcohol molecule, as shown by the ^{29}Si NMR data.

The FTIR spectrum of NP shows peaks at 2855, 2872, 2925, and 2956 cm^{-1}, which are not observed for bare silica nanoparticles. The additional peaks are also present in the spectra of 4-hydroxymethyl-*N*,*N*-dimethylbenzenamine (see Figure 2). The ratio of the intensity of the bands due to Si−OH absorption at 3400−3450 cm^{-1} and those assigned to Si−O−Si at 1100 cm^{-1} is smaller for the modified silica particles than for the bare ones. Therefore, a considerable diminution of the amount of silanol groups occurs after functionalization, as expected from the covalent bonding between the nanoparticles and the organic molecules. Any absorption due to the vibration modes assigned to Si−O−C bonds[27] is masked by the strong Si−O−Si absorption signals at 1100 cm^{-1}.

The presence of nitrogen on the surface of the particles was also confirmed by EDS and XPS experiments, as shown in Figures S1 and S3 in the Supporting Information, respectively.

Laser Flash Photolysis. The acid−base equilibria between species of the triplets of safranine-T in aqueous solution are reported in the literature[28,29] (Scheme 1). To reduce the number of species present in the system, the polar aprotic solvent acetonitrile was employed here to investigate the interaction of the triplet states of safranine-T with the modified nanoparticles.

Islam et al.[30] studied the H-abstraction process by photolysis of safranine-T in the presence of different H donors and found that a H-atom abstraction by $^3SH^+$ yields the SH_2^+ radical, which has an absorption maximum at 720 nm. The rate constant of the H-abstraction reaction from phenol in ethanol[30] is 7.7×10^5 M^{-1} s^{-1}.

If $^3SH^+$ is able to abstract a H atom from phenol (O−H bond dissociation energy (BDE) = 373 kJ mol^{-1}[31]), it might also be able to abstract a H atom from acetonitrile with a C−H BDE of a similar value (C−H BDE = 389 kJ mol^{-1}[32]).

LFP experiments at different observation wavelengths in the range from 300 to 850 nm were performed with Ar-saturated

Scheme 1. Acid−Base Equilibria between the Three Forms of the Triplet States of Safranine-T

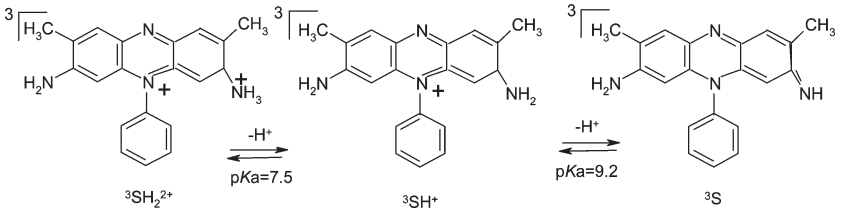

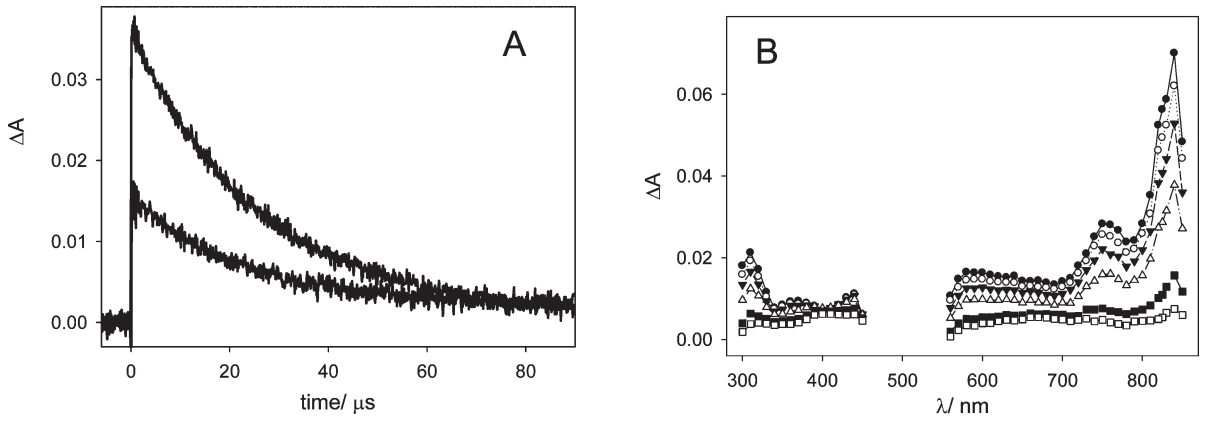

Figure 3. (A) Traces obtained at 830 nm (upper) and 730 nm (lower). (B) Experimental absorption spectra obtained with Ar-saturated 8.1×10^{-6} M safranine-T solutions in acetonitrile taken at 2 (●), 5 (○), 10 (▼), 20 (Δ), 50 (■), and 75 μs (□) after the laser shot (λ^{exc} = 532 nm).

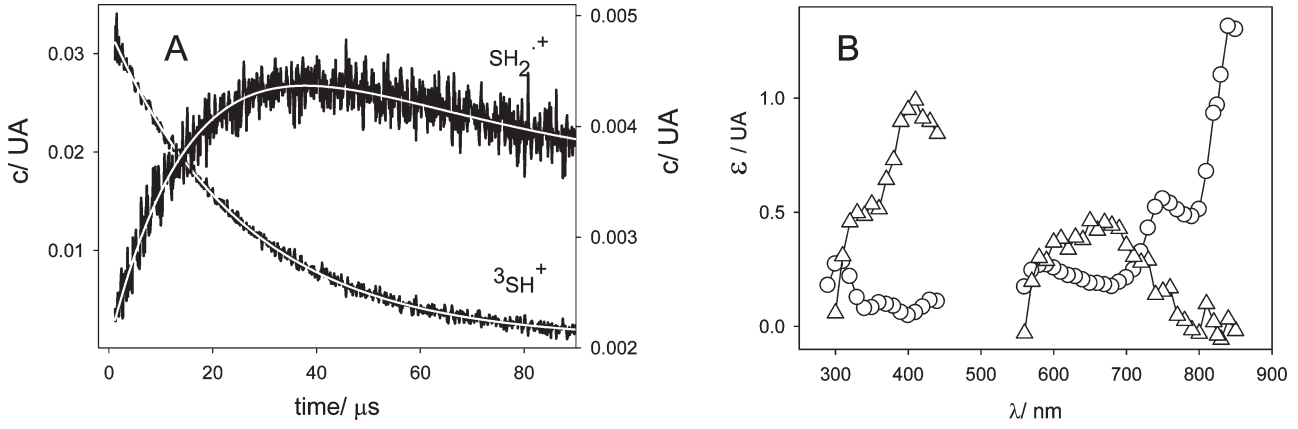

Figure 4. (A) Kinetic profiles obtained from the bilinear analysis with two species for the experiments shown in Figure 3. The white lines show fitting of the $^3SH^+$ decay to a single exponential function and fitting of the SH_2^+ kinetics to biexponential behavior. (B) Absorption spectra obtained from the bilinear analysis of the experimental data for $^3SH^+$ (○) and SH_2^+ (Δ).

solutions of safranine-T to corroborate whether this reaction takes place. The signals (Figure 3A) could be fitted to exponential decays. The absorption spectra taken at different times after the laser shot are shown in Figure 3B.

As shown in Figure 3B, the spectrum taken at 2 μs after the laser pulse is coincident with that reported for $^3SH^{+30}$ and was assigned to this species.

To obtain information on the absorption spectra and kinetics of the species involved in the experimental traces, a bilinear program was employed.[33] The analysis of the absorption matrix with the program shows that all traces can be reproduced by considering two species whose kinetic profiles and absorption spectra are shown in Figure 4A,B, respectively. Comparison of the absorption spectrum of the species formed immediately after the laser shot with that reported for $^3SH^{+30}$ supports the assignment to this triplet state. This species shows an exponential decay with an apparent rate constant of 3.8×10^4 s^{-1}. The second species is formed through the decay of $^3SH^+$, and only 10% of its maximum concentration decays within the time window of the experiment. This species (λ^{max} = 690 nm) is assigned to SH_2^+,[30] the species formed after $^3SH^+$ H-atom abstraction from acetonitrile. From the apparent rate constant obtained for the decay of $^3SH^+$ and the acetonitrile concentration (19.5 M), a bimolecular rate constant for the H-abstraction

process of 1.97×10^3 M^{-1} s^{-1} (Table 2) is obtained. These results confirm the ability of $^3SH^+$ to abstract H atoms from acetonitrile.

To better understand the behavior of the triplet states of safranine-T in suspensions of the particles, the decay of these species in solutions of benzyl alcohol derivatives was investigated. The absorption spectra taken at different times after the laser shot LFP experiments performed with Ar-saturated 8.1×10^{-6} M safranine-T solutions containing 0.288, 0.219, and 0.010 M benzyl alcohol, 4-methoxybenzyl alcohol, or DMB are shown in Figures S4 and S5 (Supporting Information) and Figure 5, respectively. The wavelength range employed for the analysis of the matrix with the bilinear program in the visible/near-infrared region (620−850 nm) was chosen to avoid absorption of the benzyl radicals[34] formed after H-abstraction from the alcohols and of the semireduced or semioxidized species of safranine-T formed by possible electron-transfer pathways (see below). The analysis of the absorption matrix with the bilinear program shows the contribution of $^3SH^+$ and SH_2^+ to the traces (results not shown). The decay kinetics of the triplet states is coincident, within the experimental error, with that of radical formation. The estimated bimolecular rate constants for the reactions of $^3SH^+$ with the alcohols are $(1.37 \pm 0.02) \times 10^4$ and $(7.1 \pm 0.3) \times 10^4$ M^{-1} s^{-1} (Table 2) for benzyl alcohol and 4-methoxybenzyl alcohol, respectively. For DMB, the reciprocal of the $^3SH^+$ lifetime monitored at 825 nm, where SH_2^+ does not absorb, linearly increases with the substrate concentration (see Figure S6 in the Supporting Information). The slope of the linear plot yields the bimolecular rate constant $k = (5.7 \pm 0.6) \times 10^7$ M^{-1} s^{-1} (Table 2) for the reaction between $^3SH^+$ and DMB.

Table 2. Bimolecular Rate Constants for the Reactions of $^3SH^+$ with Different Added Substrates (X)

added substrate (X)	$k(^3SH^+ + X)$/ M^{-1} s^{-1}
none	$(1.97 \pm 0.02) \times 10^{3a}$
benzyl alcohol	$(1.37 \pm 0.02) \times 10^4$
4-methoxy benzyl alcohol	$(7.1 \pm 0.3) \times 10^4$
DMB	$(5.7 \pm 0.6) \times 10^7$
NP	$(1.91 \pm 0.01) \times 10^9$

[a] For X = CH_3CN (see text). The error bars represent the standard deviations.

These results imply that, in the presence of the alcohols, the H-abstraction pathway, either from the solvent or from the alcohols, contributes to the decay of $^3SH^+$. From the bond dissociation energy (BDE) of the methylenic C−H bond in benzyl alcohol (331 kJ mol^{-1}[35]), it is reasonable to expect that the reactions of $^3SH^+$ with the alcohols include the H-abstraction from the methylenic C−H bond (reaction 1 in Table 3).

The decay of $^3SH^+$ in 3.1 g L^{-1} (1.3×10^{-5} M) suspensions of the bare SiO_2 nanoparticles (data not shown) was coincident with that obtained in acetonitrile solutions. This result means that any reaction of $^3SH^+$ with the silanol groups of the particles must be neglected. The absorption spectra taken at different times after the laser shot obtained from LFP experiments with 3.9 g L^{-1} (1.4×10^{-5} M) NPs suspended in safranine-T solutions are shown in Figure 5B. The absorbance increase observed around 700 nm can be assigned to SH_2^+ (λ^{max} = 720 nm).[30] A bilinear analysis in the 620−850 nm region shows that the absorption at these wavelengths can be expressed as a linear combination of two spectra, one of them coincident with that reported for $^3SH^+$ and the other assigned to SH_2^+ (see Figure 6B). The rate constants for the decay of $^3SH^+$ and for the rise time of SH_2^+ are coincident (see Figure 6A). This result implies that $^3SH^+$ is able to abstract H atoms from the organic groups of the particles (reaction 3 in Table 3). From the decay rate of SH_2^+ [$(6.50 \pm 0.03) \times 10^4$ s^{-1}] and the concentration of NPs employed (1.4×10^{-5} M), the bimolecular rate constant for the reaction of $^3SH^+$ with the NPs is $(1.91 \pm 0.01) \times 10^9$ M^{-1} s^{-1} (Table 2).

The aromatic rings of both 4-methoxybenzyl alcohol and DMB have electron donor substituents that stabilize the corresponding radical cations.[36,37] Thus, the electron transfer (reaction 2 in Table 3) must be considered as an alternative to H-abstraction.

The change of standard Gibbs energy $\Delta_{ET}G^0$ for a charge transfer reaction involving an excited triplet state can be expressed by eq 1, which relates the redox potential E_0 of the acceptor ($^3SH^+$) with that of the donor (benzyl alcohol derivatives), and the triplet energy[38] of $^3SH^+$, ΔE_{oo} in J mol^{-1}. N_A is the Avogadro constant, and e is the electron charge.

$$\Delta_{ET}G^0 = N_A \times (e \times E^0(X^+/X) - e \times E^0(^3SH^+/SH^\bullet)) - \Delta E_{oo} \quad (1)$$

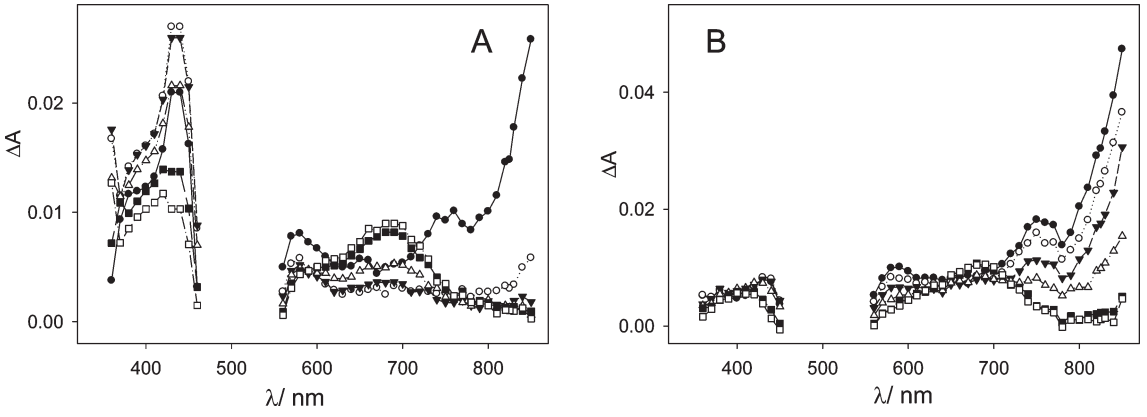

Figure 5. Experimental absorption spectra obtained with Ar-saturated 8.1×10^{-6} M safranine-T solutions in acetonitrile taken at 2 (●), 5 (○), 10 (▼), 20 (Δ), 50 (■), and 75 μs (□) after the laser shot (λ^{exc} = 532 nm) in the presence of (A) 0.010 M DMB and (B) 3.9 g L^{-1} NPs.

Table 3. H-Abstraction and Electron-Transfer Reactions Involving $^3SH^+$ and the Benzyl Alcohol Derivatives[a]

Reaction	Number
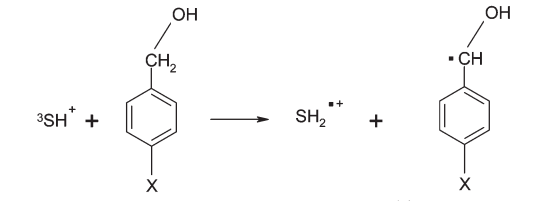	(1)
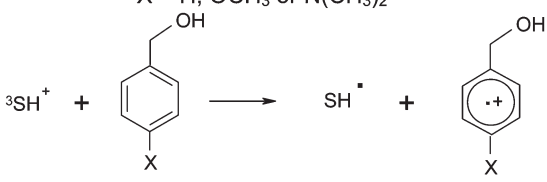	(2)
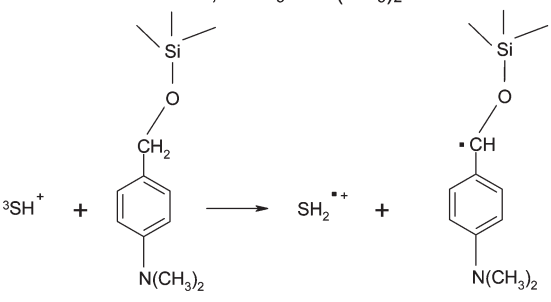	(3)
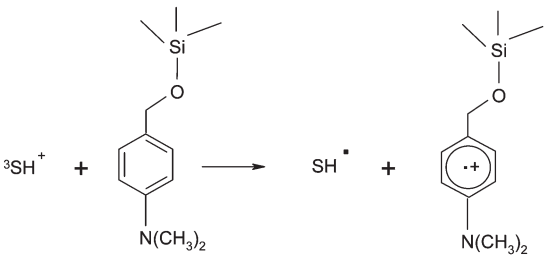	(4)

[a] For X = OCH_3, H-abstraction from the C−H bonds of the methoxy group cannot be neglected.

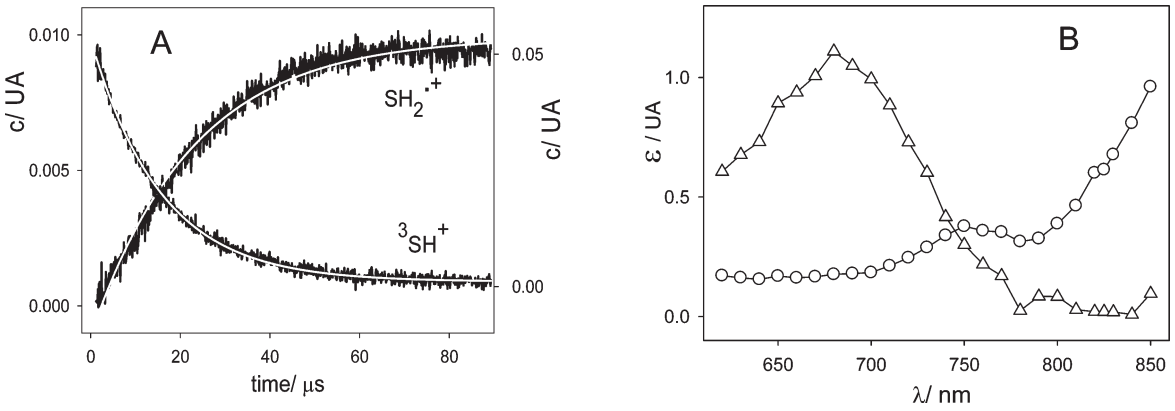

Figure 6. (A) Kinetic profiles obtained from the bilinear analysis with two species of the experiments performed with 3.9 g L^{-1} (1.4×10^{-5} M) NPs suspended in safranine-T solutions. (B) Absorption spectra obtained from the bilinear analysis of the experimental data for $^3SH^+$ (○) and SH_2^+ (Δ).

The values employed for the calculation of $\Delta_{ET}G^0$ are E^0 ($SH^+/SH^\bullet$) = (−0.35 ± 0.02) V vs NHE,[39] and ΔE_{oo} = 176.6 kJ mol^{-1}.[30] The values of E^0 (X^+/X), as well as those of $\Delta_{ET}G^0$, are listed in Table 4.

The value of E^0 (X^+/X) for DMB was obtained from the linear correlation between the literature values of E^0 (X^+/X) measured for substituted *N*,*N*-dimethylanilines in acetonitrile

dx.doi.org/10.1021/jp205112u |*J. Phys. Chem. C* 2011, 115, 18122–18130

solution[42,43] and the Hammett parameter σ_p[44] (see Figure S7 in the Supporting Information) taking $\sigma_p = -0.04$ for the CH_2OH group.[45]

For several reactions, low positive $\Delta_{ET}G^0$ values imply the existence of a reversible electron-transfer process.[46−48] In fact, although, for benzyl alcohol and 4-methoxybenzyl alcohol, the calculated values of $\Delta_{ET}G^0$ are 68 and 48 kJ mol^{-1}, respectively, the spectra taken at times ≥ 50 μs show absorption in the 400−500 nm range (see Figure 7), where both the semireduced species of safranine-T ($SH^{\bullet}$)[49] and the radical cations obtained from the alcohols[50] absorb. This result supports the existence of the electron-transfer processes depicted in reaction 2 of Table 3.

For DMB containing an excellent electron donor as a substituent in the aromatic ring,[36,37] $\Delta_{ET}G^0 = -57$ kJ mol^{-1} was obtained, which shows that the transfer is a favorable reaction route (reaction 2 in Table 3). On the basis of similar arguments employed for the other benzyl alcohol derivatives, the electron-transfer process (reaction 4 in Table 3) should also be reversible. Assuming a similar value of E^0 (X^+/X) for the amine adsorbed on the NP, a thermodynamically feasible electron transfer from the organic group of the particles to $^3SH^+$ should also be expected. Both panels A and B in Figure 5 show absorption in the 400−500 nm range at times ≥ 50 μs, which supports the existence of the electron-transfer routes in the homogeneous and heterogeneous systems (see above).

The ratio of the rate constants for particle-bound organic groups ($k_{SH,P}$) versus free-solution ($k_{SH,DMB}$) quenching gives kinetic information on the effect of immobilizing the organic compound on a surface.[7] Assuming a diffusion-controlled encounter in solution for $^3SH^+$ quenching, reactions 1−4, the ratio $k_{SH,P}/k_{SH,DMB}$ may be written as

$$\frac{k_{SH,P}}{k_{SH,DMB}} = \frac{R_{P+SH}D_{P+SH}}{R_{DMB+SH}D_{DMB+SH}n_{DMB/P}}\exp(-\Delta E_a/kT)$$

Table 4. Values of E^0 (X^+/X) and $\Delta_{ET}G^0$ for the Reactions of $^3SH^+$ with the Alcohols

	E^0 (X^+/X) (V) vs SHE	$\Delta_{ET}G^0$ (kJ mol^{-1})
benzyl alcohol	2.18[a]	68
4-methoxybenzyl alcohol	1.98[b]	48
DMB	0.89[c]	−57

[a] From ref 40. [b] From ref 41. [c] See the text.

where R_{P+SH} and R_{DMB+SH} are the sum of the radii of $^3SH^+$ (R_{SH}) and particle P (R_P), and of $^3SH^+$ and DMB (R_{DMB}), respectively. D_{P+SH} and D_{DMB+SH} are the corresponding mutual diffusion coefficients given by $D_P + D_{SH}$ and $D_{DMB} + D_{SH}$, respectively. $n_{DMB/P}$ is the number of DMB groups attached to each particle ($n_{DMB/P} = 241$), calculated as the number of silanol groups per particle multiplied by the fraction of covered silanols, f(SiOR) = 0.34 (see above).

The radii $R_{DMB} = 0.385$ nm and $R_{SH} = 0.565$ nm were determined from the energy-minimized geometries obtained from HyperChem, respectively; these values were used to estimate R_{P+SH} and R_{DMB+SH}. Because of the large size of the silica particles, the mutual diffusion coefficient for interfacial quenching is dominated by the diffusion of safranine-T, $D_{P+SH} \sim D_{SH}$, and thus, $D_{P+SH}/D_{DMB+SH} \sim R_{DMB}/(R_{DMB} + R_{SH}) = 0.41$.

The factor $\exp(-\Delta E_a/kT)$ is due to the difference in the energy barrier (ΔE_a) of the quenching reactions of $^3SH^+$ with the particle P and with DMB. ΔE_a is expected to be small, since, as shown above, triplet safranine-T reacts in a similar way toward the organic compound either free or attached to the particle, and thus $\exp(-\Delta E_a/kT) \sim 1$ will be considered.

From the previous considerations, a value of $k_{SH,P}/k_{SH,DMB} = 7 \times 10^{-3}$ is predicted. However, the observed rate constant for quenching of triplet safranine-T by the organic groups bonded to the particle was found to be 33 times larger than that by the free organic groups. Shield and Harris[7] observed that the interfacial reactions of triplet benzophenone were enhanced compared to reactions in free solution. A rate enhancement of a heterogeneous reaction can be observed if the surface plays a significant role in the frequency of encounters between reacting molecules. Interfacial reactions can occur through a direct (Eley−Rideal) and/or indirect (Langmuir−Hinshelwood) mechanism.[51]

The indirect mechanism proceeds through the adsorption of the reactant, followed by surface diffusion to a reactive site, which can result in a significant rate enhancement in comparison to the analogous reaction in free solution.[52−54] Our results indicate that quenching at the colloid/solution interface is about 3 orders of magnitude faster than the rate expected from the Eley−Rideal mechanism (see previous estimations). This suggests that an indirect mechanism is likely responsible for the enhancement of the reaction rate compared with free solution.

By using reflection second-harmonic generation (SHG), Xu et al.[55] proposed that, in silica suspensions in CH_3CN, the lone electron pair of the nitrogen atom of the solvent can reversibly accept a proton from SiOH groups at the interface to yield

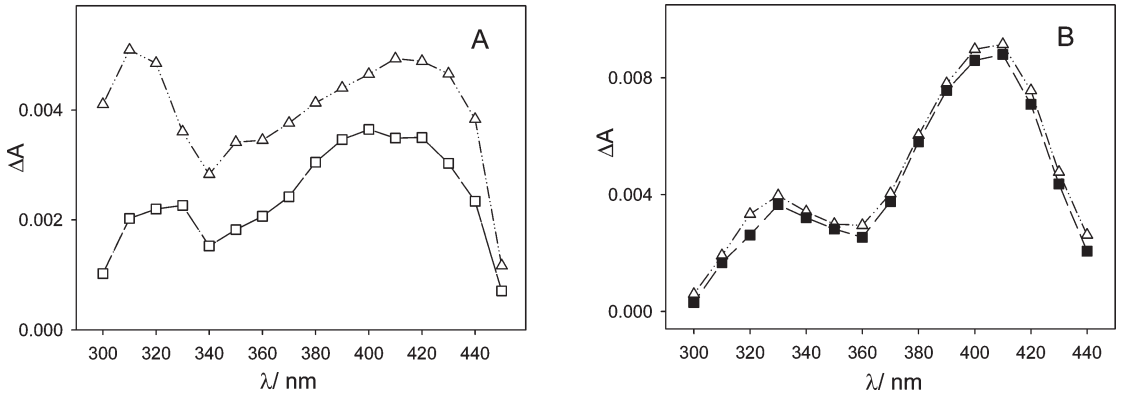

Figure 7. Experimental absorption spectra obtained with Ar-saturated safranine-T solutions taken at 50 and 75 μs after the laser shot (λ = 532 nm), in the presence of (A) benzyl alcohol and (B) 4-methoxybenzyl alcohol.

surface SiO^- groups. These deprotonated groups act as sites for the adsorption of cationic probes by Coulombic interactions. This means that the equilibrium constant for the adsorption of the cationic safranine-T on unmodified silica nanoparticles suspended in acetonitrile[8] (3.0×10^4) should be an upper limit for the equilibrium constant for the adsorption of the dye at the NP/CH_3CN surface. Thus, under our conditions, a non-negligible fraction ($\leq$30%) of the safranine-T should be adsorbed at the NP/CH_3CN surface, which supports the occurrence of an indirect mechanism.

Moreover, adsorption of safranine on hydrophobic and hydrophilic glass surfaces has been reported to obey the Langmuir equation;[6] adsorption on hydrophilic surfaces is energetically exothermic and an enthalpy-controlled process, whereas entropy change controls the endothermic adsorption on hydrophobic surface glass, indicating different adsorption forces. At room temperature, the equilibrium constant K was found to be 2240 and 1000 for hydrophobic and hydrophilic surfaces, respectively, therefore, supporting an increased reactivity between adsorbed benzyl alcohols and safranine.

CONCLUSION

Application of the bilinear analysis to the absorption matrices obtained from LFP experiments performed in the 620−850 nm range with solutions of 4-hydroxymethyl-*N*,*N*-dimethylbenzenamine, benzyl alcohol, and 4-methoxybenzyl alcohol showed the triplet safranine-T H-abstraction process from the methylenic C−H bonds in benzyl alcohol and its two derivatives. Evidence for a reversible electron transfer from the benzyl alcohol derivatives to triplet safranine-T is obtained from the absorption spectra at times $\geq$ 50 μs and from Gibbs energy calculations.

A similar analysis is employed to support the existence of the H-abstraction and electron-transfer reaction routes between triplet safranine-T and the silica nanoparticles modified with 4-hydroxymethyl-*N*,*N*-dimethylbenzenamine suspended in acetonitrile.

From the enhancement of the rates of the interfacial reactions of triplet safranine-T with the organic groups of the particles compared to those in free solution, it can be concluded that the dye is adsorbed on the silica surface, which makes this system interesting from an environmental point of view since coadsorption of dyes and alcohols on mineral particles is expected to take place in natural waters.

ASSOCIATED CONTENT

Supporting Information. TEM images, EDS spectrum, ^{29}Si NMR in solid state, XPS spectrum of the modified nanoparticles, laser flash photolysis spectra obtained with 4-methoxybenzyl alcohol solutions, dependence of the reciprocal of the safranine-T triplet state lifetime on the concentration of 4-hydroxymethyl-*N*,*N*-dimethylbenzenamine, and plot of redox potential versus Hammett parameter for substituted *N*,*N*-dimethylanilines. This material is available free of charge via the Internet at http://pubs.acs.org.

AUTHOR INFORMATION

Corresponding Author

*Phone: +54 221 4257430/7291. Fax: +54 221 4254642. E-mail: dmartire@inifta.unlp.edu.ar.

ACKNOWLEDGMENT

The authors thank Dr. F. C. Lovey and Dr. A. Condó for the TEM experiments. This work was supported by Grant PICT 2008 # 0686 from Agencia Nacional de Promoción Científica y Tecnológica, (ANPCyT, Argentina). S.G.B. and M.C.G. are research members of CONICET, Argentina. D.O.M. is a research member of Comisión de Investigaciones Científicas de la Provincia de Buenos Aires (Argentina).

REFERENCES

(1) Wiesner, M. R.; Lowry, G. V.; Jones, K. L.; Hochella, M. F.; Di Giulio, R. T.; Casman, E.; Bernhardt, E. S. *Environ. Sci. Technol.* **2009**, *43*, 6458–6462.

(2) Roco, M. C.; Bainbridge, W. S. *Societal Implications of Nanoscience and Nanotechnology*; National Science Foundation: Arlington, V.A., 2001.

(3) Chen, Y. X.; Chen, H. L.; Xu, Y. T.; Wei Shen, M. *Environ. Int.* **2004**, *30*, 31–37.

(4) Budavari, S. *Encyclopedia of Chemicals, Drugs, and Biologicals*, 11th ed.; Merck & Co., Inc.: Rahway, NJ, 1989; p 176.

(5) Preethi, S.; Sivasamy, A.; Sivanesan, S.; Ramamurthi, V.; Swaminathan, G. *Ind. Eng. Chem. Res.* **2006**, *45*, 7627–7632.

(6) Atun, G.; Hisarlı, G.; Tunçay, M. *Colloids Surf., A* **1998**, *143*, 27–33.

(7) Shield, S. R.; Harris, J. M. *J. Phys. Chem. B* **2000**, *104*, 8527–8535.

(8) Arce, V. B.; Bertolotti, S. G.; Oliveira, F. J. V. E.; Airoldi, C.; Gonzalez, M. C.; Allegretti, P. E.; Mártire, D. O. *Spectrochim. Acta, Part A* **2009**, *73*, 54–60.

(9) Brunauer, S.; Emmett, P. H.; Teller, E. *J. Am. Chem. Soc.* **1938**, *60*, 309–319.

(10) Vogel, A. I. *Textbook of Practical Organic Chemistry*, 5th ed.; John Wiley & Sons: New York, 1989.

(11) Ossenkamp, G. C.; Kemmitt, T.; Johnston, J. H. *Langmuir* **2002**, *18*, 5749–5754.

(12) Ossenkamp, G. C.; Kemmitt, T.; Johnston, J. H. *Chem. Mater.* **2001**, *13*, 3975–3980.

(13) Ruiz, A. E.; Caregnato, P.; Arce, V. B.; Schiavoni, M. M.; Mora, V. C.; Gonzalez, M. C.; Allegretti, P. E.; Mártire, D. O. *J. Phys. Chem. C* **2007**, *111*, 7623–7628.

(14) Arce, V. B.; Rosso, J. A.; Oliveira, F. J. V. E.; Airoldi, C.; Soria, D. B.; Gonzalez, M. C.; Allegretti, P. E.; Mártire, D. O. *Photochem. Photobiol.* **2010**, *86*, 1208–1214.

(15) Bertolotti, S. G.; Previtali, C. M. *J. Photochem. Photobiol., A* **1997**, *103*, 115–119.

(16) Badhah, S.; Airoldi, C. *Chem. Eng. J.* **2011**, *166*, 420–427.

(17) Macedo, T. M.; Airoldi, C. *Dalton Trans.* **2009**, 7402–7409.

(18) Jitianu, A.; Crisan, A.; Meghea, A.; Raub, I.; Zaharescua, M. J. *Mater. Chem.* **2002**, *12*, 1401–1407.

(19) Fryxell, G. E.; Lin, Y.; Fiskum, S.; Birnbaum, J. C.; Wu, H.; Kemner, K.; Kelly, S. *Environ. Sci. Technol.* **2005**, *39*, 1324–1331.

(20) Makkuni, A.; Varma, R. S.; Sikdar, S. K.; Bhattacharyya, D. *Clean Technol. Environ. Policy* **2005**, *7*, 87–96.

(21) Silva, A. L. P.; Sousa, K. S.; Germano, A. F. S.; Oliveira, V. V.; Espínola, J. G. P.; Fonseca, M. G.; Airoldi, C.; Arakaki, T.; Arakaki, L. N. H. *Colloids Surf., A* **2009**, *332*, 144–149.

(22) Jal, P. K.; Patel, S.; Mishra, B. K. *Talanta* **2004**, *62*, 1005–1028.

(23) Kammler, H. K.; Beaucage, G.; Mueller, R.; Pratsinis, S. E. *Langmuir* **2004**, *20*, 1915–1921.

(24) Zhuralev, L. T. *Colloids Surf., A* **2000**, *173*, 1–38.

(25) Farias, R. F.; Airoldi, C. *J. Therm. Anal.* **1998**, *53*, 751–756.

(26) Sales, J. A. A.; Petrucelli, G. C.; Oliveira, F. J. V. E.; Airoldi, C. *J. Colloid Interface Sci.* **2006**, *297*, 95–103.

(27) Llansola Portolés, M. J.; Rodríguez Nieto, F.; Soria, D. B.; Amalvy, J. I.; Peruzzo, P. J.; Mártire, D. O.; Kotler, M. O.; Holub, O.; Gonzalez, M. C. *J. Phys. Chem. C* **2009**, *113*, 13694–13702.

(28) Borsarelli, C.; Bertolotti, S. G.; Previtali, C. M. *Photochem. Photobiol. Sci.* **2002**, *1*, 574–580.

(29) Encinas, M. V.; Previtali, C. M.; Bertolotti, S. G.; Neumann, M. G. *Photochem. Photobiol.* **1995**, *62*, 65–70.
(30) Islam, S. D. M.; Fujitsuka, M.; Ito, O. *Phys. Chem. Chem. Phys.* **1999**, *1*, 3737–3742.
(31) da Silva, G.; Chen, C. C.; Bozzelli, J. W. *Chem. Phys. Lett.* **2006**, *424*, 42–45.
(32) Goebbert, D. J.; Velarde, L.; Khuseynov, D.; Sanov, A. *J. Phys. Chem. Lett.* **2010**, *1*, 792–795.
(33) San Román, E. A.; Gonzalez, M. C. *J. Phys. Chem.* **1989**, *93*, 3532–3536.
(34) Sehested, K.; Corfltzen, H.; Christensen, H. C.; Hart, E. J. *J. Phys. Chem.* **1975**, *79*, 310–315.
(35) Brandi, P.; Galli, C.; Gentili, P. *J. Org. Chem.* **2005**, *70*, 9521–9528.
(36) Holcman, J.; Sehested, K. *J. Phys. Chem.* **1976**, *80*, 1642–1644.
(37) Rosso, J. A.; Caregnato, P.; Mora, V. C.; Gonzalez, M. C.; Mártire, D. O. *Helv. Chim. Acta* **2003**, *86*, 2509–2524.
(38) Braslavsky, S. E. *Pure Appl. Chem.* **2007**, *79*, 293–465.
(39) Guha, S. N.; Mittal, J. P. *Faraday Trans.* **1997**, *93*, 3647–3652.
(40) Fukuzumi, S.; Itoh, S.; Komori, T.; Suenobu, T.; Ishida, A.; Fujitsuka, M.; Ito, O. *J. Am. Chem. Soc.* **2000**, *122*, 8435–8443.
(41) Fabbrini, M.; Galli, C.; Gentili, P. *J. Mol. Catal. B* **2002**, *16*, 231–240.
(42) Baciocchi, E.; Bietti, M.; Ercolani, G.; Steenken, S. *Tetrahedron* **2003**, *59*, 613–618.
(43) Baciocchi, E.; Calcagni, A.; Lanzalunga, O. *J. Org. Chem.* **2008**, *73*, 4110–4115.
(44) Domingo, L. R.; Pérez, P.; Contreras, R. *J. Org. Chem.* **2003**, *68*, 6060–6063.
(45) Whittle, C. E. Electron transfer within various organometallic species. Ph.D. Thesis, University of Florida, Gainesville, FL, 2000.
(46) Girault, J. P.; Dana, G. *J. Chem. Soc., Perkin Trans. 2* **1977**, 993–994.
(47) Ruiz, G.; Rodríguez Nieto, F.; Wolcan, E.; Féliz, M. R. *J. Photochem. Photobiol., A* **1997**, *107*, 47–54.
(48) Mártire, D. O.; Gonzalez, M. C. *J. Phys. Org. Chem.* **2000**, *13*, 208–212.
(49) Baumgartner, C. E.; Richtol, H. H.; Aikens, D. A. *Photochem. Photobiol.* **1981**, *34*, 17–22.
(50) Johnston, L. J.; Wayner, D. M.; Parker, V. D. *J. Am. Chem. Soc.* **1994**, *116*, 8279–8287.
(51) Demeter, A.; Berces, T. *J. Photochem. Photobiol., A* **1989**, *46*, 27–40.
(52) Yekta, A.; Turro, N. J. *Mol. Photochem.* **1972**, *3*, 307–322.
(53) Demeter, A.; Berces, T. *J. Phys. Chem.* **1991**, *95*, 1228–1232.
(54) Naguib, Y. M. A.; Cohen, S. G.; Steel, C. *J. Am. Chem. Soc.* **1986**, *108*, 128–133.
(55) Xu, Z.; Li, J.; Dong, Y. *Langmuir* **1998**, *14*, 1183–1188.